ACTA NEUROBIOLOGIAE EXPERIMENTALIS

Research paper Acta Neurobiol Exp 2010, 70: 1–12

Spatial and temporal changes of osteopontin in oxygen–glucose-deprived hippocampal slice cultures

Ji-Yeon Lee, Jeong-Sun Choi, Jae-Youn Choi, Yoo-Jin Shin, Hou Yun, Jung-Ho Cha, Myung-Hoon Chun, and Mun-Yong Lee*

Department of Anatomy, College of Medicine, The Catholic University of Korea, Seoul, Korea, *Email: munylee@catholic.ac.kr

We have examined the temporal changes and cellular localization of osteopontin (OPN) mRNA and protein in organotypic hippocampal slice cultures subjected to ischemia-like oxygen–glucose deprivation (OGD). The sequential induction pattern of OPN expression occurred in a time- and cell-dependent manner in hippocampal slice cultures after OGD. The early response consisted of neuronal and microglial OPN upregulation, followed by a later extended phase of expression in reactive astrocytes. OPN immunoreactivity after OGD matched the mRNA induction patterns. Activated microglia revealed OPN staining in focal deposits, whereas neurons and reactive astrocytes showed perinuclear staining with a punctate cytosolic pattern of OPN, typical of secreted proteins. These data demonstrated that the temporal and cellular patterns of OPN induction in reactive glial cells in this *in vitro* model closely correlated with that in the *in vivo* model, suggesting that OPN has a multifunctional role in the pathogenesis of ischemic injury.

Key words: organotypic hippocampal slice cultures, oxygen-glucose-deprivation, osteopontin, microglia, reactive astrocyte, neurons

INTRODUCTION

Osteopontin (OPN) is a multifunctional acidic glycoprotein that is linked to a variety of pathophysiological processes in the nervous system. In particular, the role of OPN during ischemia has been studied extensively (Ellison et al. 1998, 1999, Wang et al. 1998, Lee et al. 1999, Schroeter et al. 2006, Choi et al. 2007). OPN is believed to have neuroprotective effects against ischemic injury (Meller et al. 2005, Doyle et al. 2008). In contrast, it is implicated as a pathogenic factor involved in the activation of inflammatory microglia in Parkinson's disease (Maetzler et al. 2007), showing the ambiguity related to the role of OPN in neurodegenerative diseases.

We recently reported that two phases of OPN induction occur in a time- and cell-dependent manner in the ischemic hippocampus; i.e., an early phase of acute microglial expression and a delayed phase characterized by a strong and persistent induction of OPN in reactive astrocytes, which is likely to reflect its multifunctional role during the early and delayed phases after ischemic injury (Choi et al. 2007, Kang et al. 2008). Therefore, the role of OPN in the ischemic brain seems to be dependent on the time that has elapsed after ischemic injury and thus requires further investigation.

Organotypic hippocampal slice cultures (OHC) combined with oxygen–glucose deprivation (OGD) offer great advantages in that they closely mimic the situation that occurs in animals subjected to transient cerebral ischemia (for review, see Noraberg et al. 2005). These cultures therefore provide a convenient model system for examining OPN effects after ischemic insults.

The objective of this study was to examine the temporal changes and cellular localization of OPN mRNA and protein in hippocampal slice cultures subjected to ischemia-like OGD using *in situ* hybridization and immunohistochemistry and to compare these expression profiles with those occurring in an *in vivo* model of transient forebrain ischemia. This study should validate this *in vitro* model of stroke for ongoing studies of OPN effects in neurodegenerative diseases.

Correspondence should be addressed to M.Y. Lee, Email: munylee@catholic.ac.kr

Received 26 September 2009, accepted 12 January 2010

METHODS

Animal preparation

All experimental animal procedures were conducted with the approval of the Catholic Ethics Committee of the Catholic University of Korea, and were in accordance with the U.S. National Institutes of Health Guide for the Care and Use of Laboratory Animals (NIH Publication No. 80–23, revised 1996).

Hippocampal slice cultures were prepared according to the method of Stoppini and others (1991). Briefly, slice cultures were prepared from seven-day-old Sprague Dawley rat pups (Gapyeong, Korea). Animals were anesthetized with 4% chloral hydrate before decapitation and hippocampi were dissected and cut into 400 μm transverse sections with a McIlwain tissue chopper (The Mickle Laboratory Engineering, Guildford, UK). Hippocampal slices were placed into sterile 0.4 μm porous Millicell membranes (Millipore, Molsheim, France) in 6-well culture plates containing medium consisting of 50% minimal essential medium (Gibco–Invitrogen, Carlsbad, CA, USA), 25% horse serum (Gibco–Invitrogen), 23% Eagle's balanced salt solution (Gibco–Invitrogen) with 6.5 mg/ml glucose and HEPES (pH 7.15). Cultures were maintained at 37°C under room air and 5% CO_2 and medium was changed twice a week. Hippocampal slices were selected with the fluorescent dye, propidium iodide (PI; Molecular Probes, Eugene, OR, USA), which stains DNA in cells with a damaged plasma membrane, before the experiment. PI was added to the culture medium (0.5 μg/ml) for 24 h, and PI-negative slices were selected using a fluorescent microscope (Carl Zeiss Co., Ltd., Germany) to verify that the slices were healthy prior to insult exposure.

The induction of OGD to mimic ischemic injury was based on the method described by Laake and colleagues (1999) in serum-free "hypoglycemic" medium, Dulbecco's Modified Eagle's Medium (DMEM)-free glucose (D5030; Sigma-Aldrich, St Louis, MO, USA) supplemented with 1 mM D-glucose and 2 mM L-glutamine. This hypoglycemic medium was saturated for 1 h at 37°C in a humidified hypoxic chamber with a gas mixture containing 95% N_2/5% CO_2. After 10 days in culture, hippocampal slices were placed into hypoglycemic medium in the hypoxic chamber for 40 min. Control cultures were maintained for the same time under normoxic atmosphere in DMEM medium supplemented with 5 mM D-glucose and 2 mM L-glutamine for 40 min. For evaluation of neuronal damage, PI was added to the culture medium (5 μg/ml) during the last 2 h of reperfusion.

Semi-quantitative reverse transcriptase–polymerase chain reaction (RT–PCR)

Semiquantitative RT–PCR of organotypic slices was performed, as described in detail previously (Choi et al. 2007). After obtaining the fluorescent images, total RNA was extracted from four hippocampal slices per rat pooled for each time point after OGD using TRIzol reagent (Invitrogen, Carlsbad, CA, USA). First-strand cDNA was synthesized using Reverse Transcriptase M-MLV (Takara Korea Biomedical Inc., Korea) according to the manufacturer's instructions. Equal amounts (1 μl) of the reverse transcription products were then PCR amplified using Perfect Premix Version 2.1 (Ex Taq version; Takara Korea Biomedical Inc.). Amplification started with denaturation at 94°C for 4 min followed by 25–30 cycles of 94°C for 30 s, 58°C for 30 s and 72°C for 30 s. One picomole of each primer, using primers specific for OPN (sense, 5′-ATGAATCTGATGAGTCCTTCACTG-3′, nucleotides 426–450; antisense, 5'-GCGGAATTTCAGATAC-CTATCATC-3′, nucleotides 967–991) based on the rat OPN sequence (GenBank accession no. M14656.1), was used in the amplification reaction. Ten microliters of each PCR reaction product were electrophoresed on 1.5% (w/v) agarose gels containing ethidium bromide (1 μg/μl). For the semiquantitative measurements, we coamplified the OPN mRNA with glyceraldehyde-3-phosphate dehydrogenase (GAPDH) mRNA (GenBank accession no. M17701; sense, 5′-cgatcccgctaacatcaaat-3′, nucleotides 264 – 283; antisense, 5'-ccacagtcttctgagtg-gca-3′, nucleotides 570–589) and RT-PCR products were quantified by photographic densitometry of ethidium bromide-stained agarose gels using Quantity one® (version 4.6.3; Bio-Rad Lab., Hercules, CA, USA), with the calculated OPN/GAPDH product providing indices of OPN mRNA expression. Four hippocampal slices per rat were used for PCR, and each experimental group consisted of three rats. The data were expressed as a percentage of sham-OGD controls. Statistical significance was analyzed by analysis of variance (ANOVA) followed by Dunnett's *t*-test; $P<0.05$ was regarded as significant.

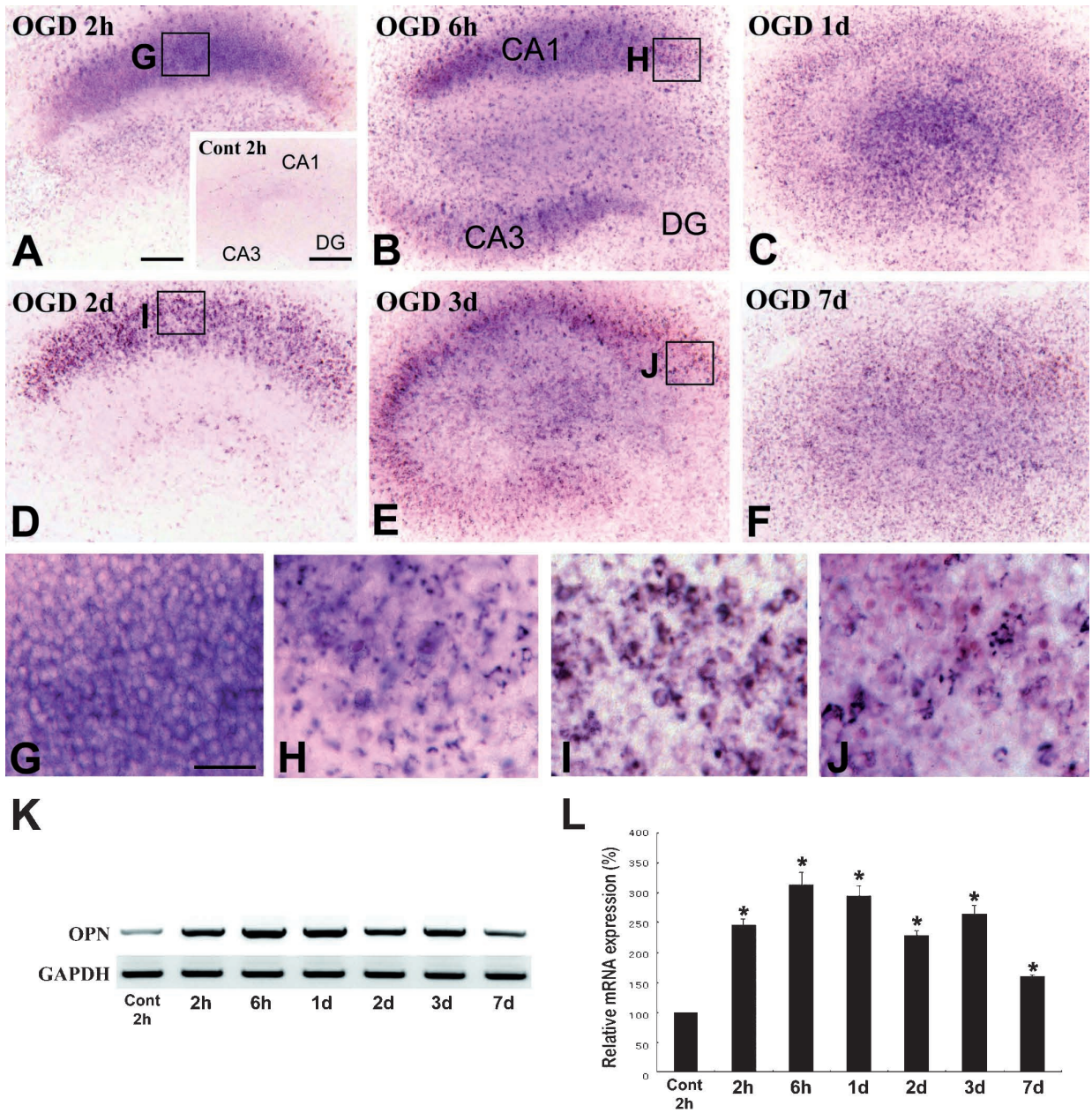

Fig. 1. Temporal changes of OPN expression in organotypic hippocampal slice cultures under control and OGD conditions. (A) At 2 h after OGD, OPN mRNA significantly increased in CA1 pyramidal neurons. At 2 h after sham-OGD, however, no significant basal expression of OPN transcripts was detected in the hippocampus (inset in A). (B) At 6 h after OGD, OPN expression was observed in CA1 and CA3 pyramidal neurons, and in scattered cells over the CA1 and CA3 neurons. DG, the dentate gyrus. (C) At 24 h after OGD, OPN expression was diffuse in CA1 and CA3 regions, and most conspicuous in the dentate hilar region. (D) At day 2 after OGD, OPN expression was exclusively localized in the CA1 pyramidal cell layer. (E) At day 3 after OGD, OPN expression was observed preferentially in the CA1 and CA3 pyramidal cell layer and the dentate hilar region. (F) At day 7 after OGD, diffuse OPN labeling was observed throughout the hippocampus. (G)–(J) Higher magnification views of the boxed areas in A, B, D, and E, respectively. (K) Semiquantitative reverse transcriptase–polymerase chain reaction analysis showed that OGD caused an upregulation of OPN mRNA in hippocampal slices compared with control slices. As an internal standard, glyceraldehyde 3-phosphate dehydrogenase (GAPDH) mRNA was measured. (L) Quantification of the intensities of RT–PCR products normalized with GAPDH mRNA. Results are expressed as a percentage of sham-OGD controls. *P<0.05 *versus* controls. Scale bar is 400 μm for inset in (A); 200 μm for (A)–(F); and 50 μm for (G)–(J).

In situ hybridization histochemistry and double labeling

Antisense and sense riboprobes labeled with digoxigenin (DIG) and specific for OPN were prepared using RT/PCR and *in vitro* transcription, as described in detail previously (Choi et al. 2007). Briefly, hippocampal slices were submersion-fixed in 4% paraformaldehyde in 0.1 M phosphate buffer (pH 7.4) for 4 h at 4°C, and were hybridized with antisense or sense probes diluted in hybridization solution (150 ng/ml) at 52°C for 18 h. Hybridization was visualized using an alkaline phosphatase-conjugated sheep anti-DIG antibody (Roche, Germany; dilution 1:2 000) with 4-nitroblue tetrazolium chloride (0.35 mg/mL) and 5-bromo-4-chloro-3-indolyl phosphate (0.18 mg/mL) as substrates.

After hybridization, as described above, some sections were incubated with biotin-conjugated mouse monoclonal anti-DIG antibody (Jackson Immuno-Research, West Grove, PA, USA; dilution 1:500) at 4°C overnight. For double-immunofluorescence histochemistry, sections were incubated at 4°C overnight with following antibodies; monoclonal mouse anti-glial fibrillary acidic protein (GFAP; Chemicon International Inc., Temecula, CA, USA; dilution 1:500), polyclonal rabbit anti-ionized calcium-binding adaptor molecule-1 (Iba-1; Wako Pure Chemical Industries, Ltd., Osaka, Japan; dilution 1:400), and monoclonal mouse anti-neuronal nuclear antigen (NeuN; Chemicon International Inc.; dilution 1:500). Antibody staining was visualized with the following secondary antibodies; Cy3-conjugated streptavidin (Jackson Immuno-Research; dilution 1:1 500) and FITC-conjugated anti-mouse antibody (Jackson ImmunoResearch; dilution 1:50). In controls, the primary antibody was omitted from the incubation solution. Counterstaining of cell nuclei was carried out by incubating the sections with DAPI (4,6-diamidino-2-phenyindole; Roche; dilution 1:1 000) for 10 min. Slides were viewed with a confocal microscope (LSM 510 Meta; Carl Zeiss Co., Ltd., Germany) equipped with three lasers. Images were converted to TIFF format, and contrast levels adjusted using Adobe Photoshop v. 7.0 (Adobe Systems, San Jose, CA, USA).

Immunoblot analysis

For immunoblot analysis, four hippocampal slices per rat pooled for each time point after OGD were homogenized in ice-cold RIPA buffer (50 mM Tris buffer, pH 8.0; 150 mM NaCl; 1% NP-40; 0.5% deoxycholate; and 0.1% SDS). Equal amounts (30 μg) of total protein from the hippocampal tissue were separated in 8% or 10% SDS–polyacrylamide gel electrophoresis (PAGE) and blotted onto cellulose membranes. Immunostaining of the blots was performed using a mouse monoclonal antibodies to OPN (Santa Cruz Biotechonolgy, Inc., Santa Cruz, CA, USA; dilution 1:500). The bands were developed with an enhanced chemiluminescence system (ECL kit, Amersham, Arlington Heights, IL, USA). Four hippocampal slices per rat were used for immunoblot analysis, and each experimental group consisted of three rats.

Densitometric analysis was performed using the Eagle Eye TMII Still Video System (Stratagene, La Jolla, CA, USA). The data were expressed as a percentage of sham-OGD controls. Statistical significance was analyzed by analysis of variance (ANOVA) followed by Dunnett's *t*-test; $P<0.05$ was regarded as significant.

Single- and double-labeling immunofluorescence

Hippocampal slices were processed for OPN immunofluorescence. After blocking with 10% normal donkey serum for 1 h, the sections were incubated with overnight at 4°C with a mouse monoclonal anti-rat OPN antibody (American Research Products, MA, USA; dilution 1:100). Primary antibody binding was visualized using Cy3-conjugated goat anti-mouse IgG (Jackson ImmunoResearch; dilution 1:500). The specificity of OPN immunoreactivity was confirmed by the absence of immunohistochemical reactions in sections from which the primary antibody had been omitted, or in which nonspecific mouse IgG was substituted.

Sections for double-immunofluorescence labeling were incubated overnight at 4°C in the presence of a mouse monoclonal antibody to OPN plus one of following antibodies; polyclonal rabbit anti-GFAP (Chemicon International; dilution 1:500), polyclonal rabbit anti-Iba-1 (dilution 1:400), and biotin-conjugated mouse monoclonal anti-NeuN (Chemicon International Inc.; dilution 1:100). The sections were then incubated with a mixture of Cy3-conjugated goat anti-mouse IgG (Jackson ImmunoResearch; dilution 1:500) and either FITC-conjugated goat anti-rabbit IgG (Jackson ImmunoResearch; dilution 1:500) or FITC-conjugated anti-biotin IgG (Jackson ImmunoResearch; dilution 1:500) for 2 h at room temperature. Control sections

were prepared as described above. Counterstaining of cell nuclei was carried out by incubating the sections with DAPI for 10 min. Slides were viewed with a confocal microscope.

RESULTS

Temporal profile of OPN mRNA expression in OHC following OGD

A brief ischemic injury (40 min OGD) followed by reperfusion under normoxic conditions resulted in the significant upregulation of OPN expression in OHC. In cultures submersed in normal non-OGD medium at all time points, no significant basal expression of OPN transcript was detected in the hippocampus (inset in Fig. 1A), as observed previously *in vivo* (Lee et al. 1999, Choi et al. 2007). At 2 h after OGD, the signal for OPN mRNA was significantly increased in CA1 pyramidal neurons; however, the signal was absent in CA3 neurons (Fig. 1A, G). Adjacent slice sections were routinely processed for *in situ* hybridization with the OPN sense probe and no specific cellular labeling was present (data not shown). At 6 h after OGD, a further increase in OPN expression appeared and spread into the CA3 pyramidal neurons (Fig. 1B). Additional labeling was detected in scattered cells over the CA1 and CA3 pyramidal neurons (Fig. 1H). At day 1 after OGD, the signals over the pyramidal neurons were absent; however, diffuse OPN expression was observed in CA1 and CA3 regions and was most conspicuous in the dentate hilar region (Fig. 1C). At day 2 after OGD,

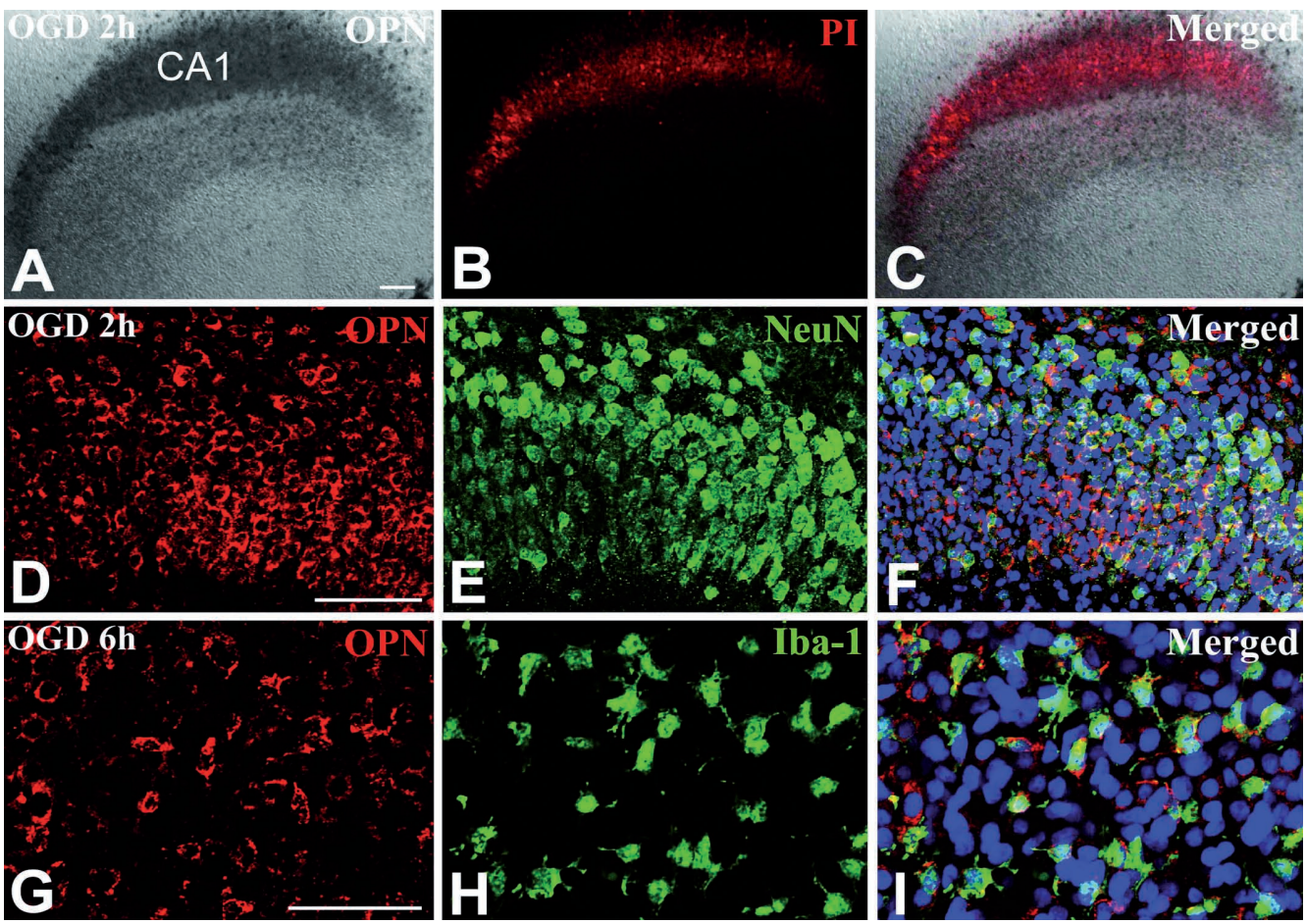

Fig. 2. Identification of phenotypes of OPN-expressing cells in organotypic hippocampal slice cultures at 2 h (A)–(F) or 6 h (G)–(I) after OGD. (A)–(F) Double labeling for OPN (A, D) and PI (B) or NeuN (E) showed that OPN expression in the CA1 pyramidal cell layer overlapped with that of PI staining, and these cells were NeuN-immunoreactive neurons. (G)–(I) Double labeling for OPN mRNA (G) and Iba-1 (H) revealed that many OPN expressing cells in the CA1 pyramidal cell layer were activated microglial cells. Note that OPN-labeled cells demonstrating morphology of CA1 neurons were negative for Iba-1. Scale bar is 200 μm for (A)–(C); 100 μm for (D)–(F); 50 μm for (G)–(I).

OPN expression was localized almost exclusively in the CA1 pyramidal cell layer, where the signal was observed in round cells resembling amoeboid-activated microglia (Fig. 1D, I). At day 3 after OGD, OPN expression had increased preferentially in the CA1 and CA3 pyramidal cell layer and the dentate hilar region (Fig. 1E). As shown at higher magnification in Fig. 1J, the signals were localized in irregular-shaped cell bodies, which differed from that observed at day 2 after OGD. At day 7 after OGD, diffuse labeling was observed throughout the hippocampus (Fig. 1F). Semiquantitative RT–PCR analysis showed that OGD

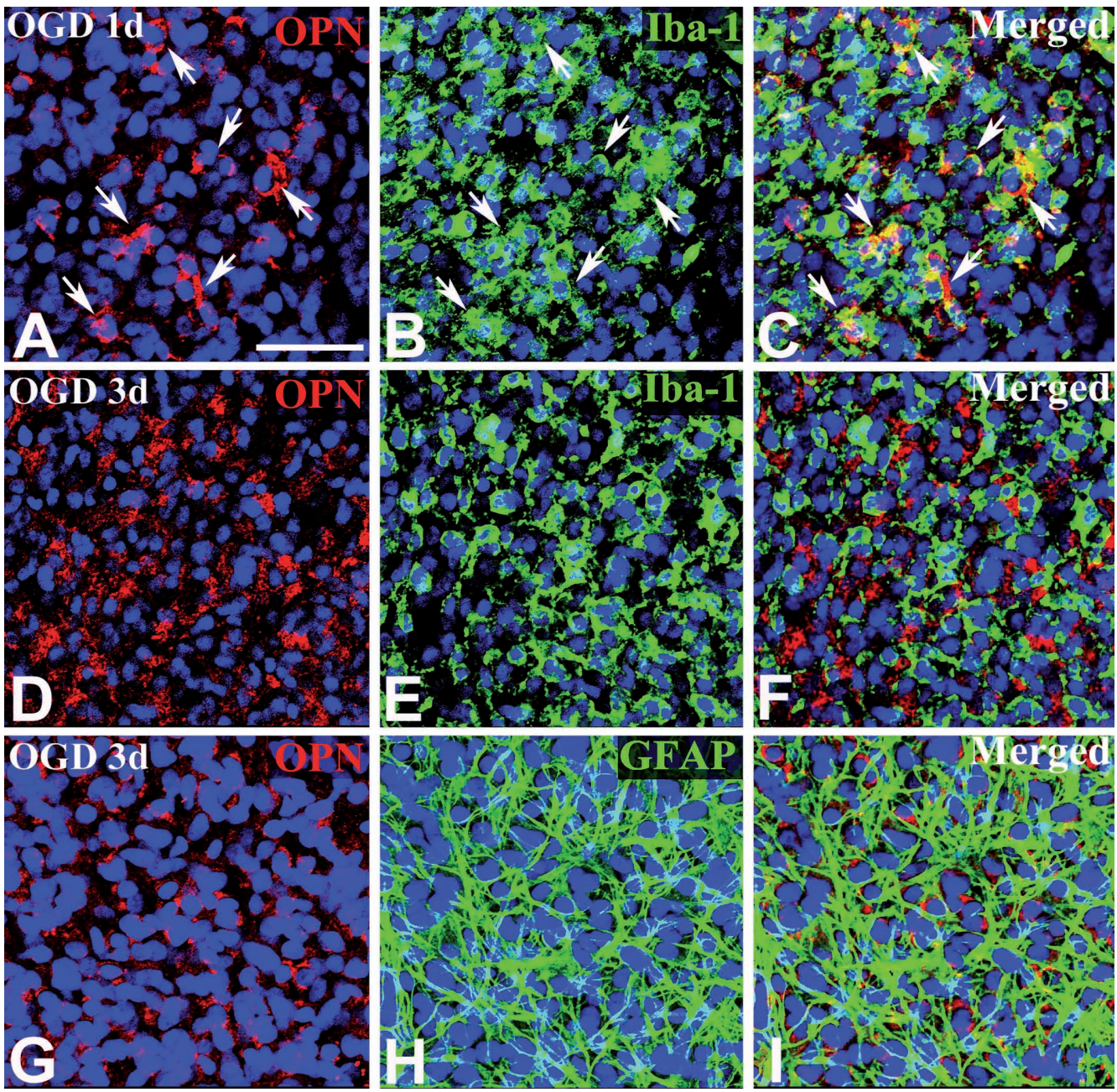

Fig. 3. Identification of phenotypes of OPN-expressing cells in organotypic hippocampal slice cultures at day 1 [(A)–(C)] or day 3 [(D)–(I)] after OGD. Double labeling for OPN [(A), (D), (G)] and Iba-1 [(B), (E)] or GFAP (H) in the CA1 pyramidal cell layer. At day 1 after OGD, most OPN-expressing cells were microglial cells that also stained positive for Iba-1 [arrows in (A)–(C)]. At day 3 after OGD, however, most OPN-labeled cells were positive for GFAP and negative for Iba-1. Scale bar is 50 μm for (A)–(I).

caused an upregulation of OPN mRNA in hippocampal slices compared with control hippocampal slices (Fig. 1K). This increase was detected as early as 2 h after OGD, reached a peak at 6 h, and then declined up to day 2. However, levels of OPN mRNA slightly increased at day 3 and this enhanced expression was maintained up to day 7, which was the latest time point examined (Fig. 1L).

The phenotype of OPN mRNA expressing cells in OHC following OGD

Confocal microscopy of double-stained slices was used to more rigorously determine the cells in which OPN was induced. At 2 h after OGD, OPN expression in the CA1 pyramidal cell layer overlapped with PI uptake (Fig. 2A–C), and this expression pattern was maintained in the CA1 and CA3 pyramidal cell layers at 6 h after OGD (data not shown). Double labeling with OPN mRNA and NeuN in the CA1 region at 2 h after OGD revealed that most OPN-expressing cells coexpressed NeuN (Fig. 2D–F). At 6 h after OGD, however, double-labeling for OPN mRNA and Iba-1, a novel microglial marker, or NeuN, revealed that many OPN-expressing cells were activated microglial cells (Fig. 2G–I), in addition to OPN/NeuN double-labeled CA1 neurons (data not shown).

In slices at day 1 after OGD, double labeling for OPN mRNA and Iba-1 or GFAP in the CA1 region revealed that most OPN-expressing cells were positive for Iba-1 (Fig. 3A–C), but not for GFAP (data not shown). At this time point, however, no OPN expression was observed in preserved pyramidal neurons showing NeuN immunoreactivity (data not shown). At day 2 after OGD, OPN expression was also localized in Iba-1-immunoreactive cells, which were large round amoeboid-like brain macrophages in the CA1 pyramidal cell layer (data not shown). In contrast, double-labeling with OPN mRNA and GFAP or Iba-1 in the CA1 region three days after OGD showed that OPN expression was no longer associated with Iba-1-immunoreactive cells (Fig. 3D–F); however, most OPN-expressing cells were positive for GFAP (Fig. 3G–I).

Temporal profile of OPN protein in OHC following OGD

The spatiotemporal distribution pattern of OPN protein closely matched that of OPN mRNA. In agreement with *in situ* hybridization histochemistry, no clear immunoreactivity for OPN could be seen in cultures submersed in normal non-OGD medium at all time points (Fig. 4A). A brief ischemic injury (40 min OGD) followed by reperfusion under normoxic conditions resulted in the significant upregulation of OPN protein expression in OHC. Weak OPN-labeled profiles were visible in CA1 pyramidal cell layer at 2 h after OGD, and spread into the CA3 pyramidal cell layer at 6 h after OGD (Fig. 4B). In addition, more intensely labeled profiles with the OPN concentrated in focal deposits were evident in the CA1 region at 6 h after OGD (Fig. 4B). The latter signals had increased preferentially in the CA1 and the dentate hilar regions by 1 day (Fig. 4C) and 2 days (data not shown). At day 3 after OGD, OPN-labeled cells exhibited perinuclear staining with a punctate cytosolic pattern of OPN, which appeared to be different from cells that observed at early phase after OGD (Fig. 4D). At day 7 after OGD, the labeling pattern was similar to those seen at three days after OGD (data not shown).

Immunoblotting with specific antibody against OPN revealed that a major band was located at molecular weight between 50 and 75 kDa (Shin et al. 2005). Relative protein expression in the major band was increased in the hippocampal slices after OGD compared with control hippocampal slices (Fig. 4E). This increase was detected as early as 2 h after OGD, reached a peak at 1 day, and then declined up to day 2. However, enhanced expression of OPN was maintained up to day 7, which was the latest time point examined (Fig. 4F).

The phenotype of OPN-immunoreactive cells in OHC following OGD

To define the cell phenotype expressing OPN protein in OHC following OGD, we performed double-labeling using markers of neuronal or glial markers, such as NeuN, Iba-1 and GFAP. Double labeling with OPN and NeuN in the CA1 region at 6 h after OGD revealed that weak OPN immunoreactivity appeared to localize diffusely in the neuronal cell body (Fig. 5A–C). However, cells showing OPN staining in focal sites were not associated with NeuN immunoreactive neurons. At 1 day after OGD, double-labeled immunofluorescence showed that cells with the OPN concentrated in focal deposits were indeed Iba-1-immunoreactive microglial cells (Fig. 5D–F). In contrast, double-labeling for OPN and GFAP in the CA1 region

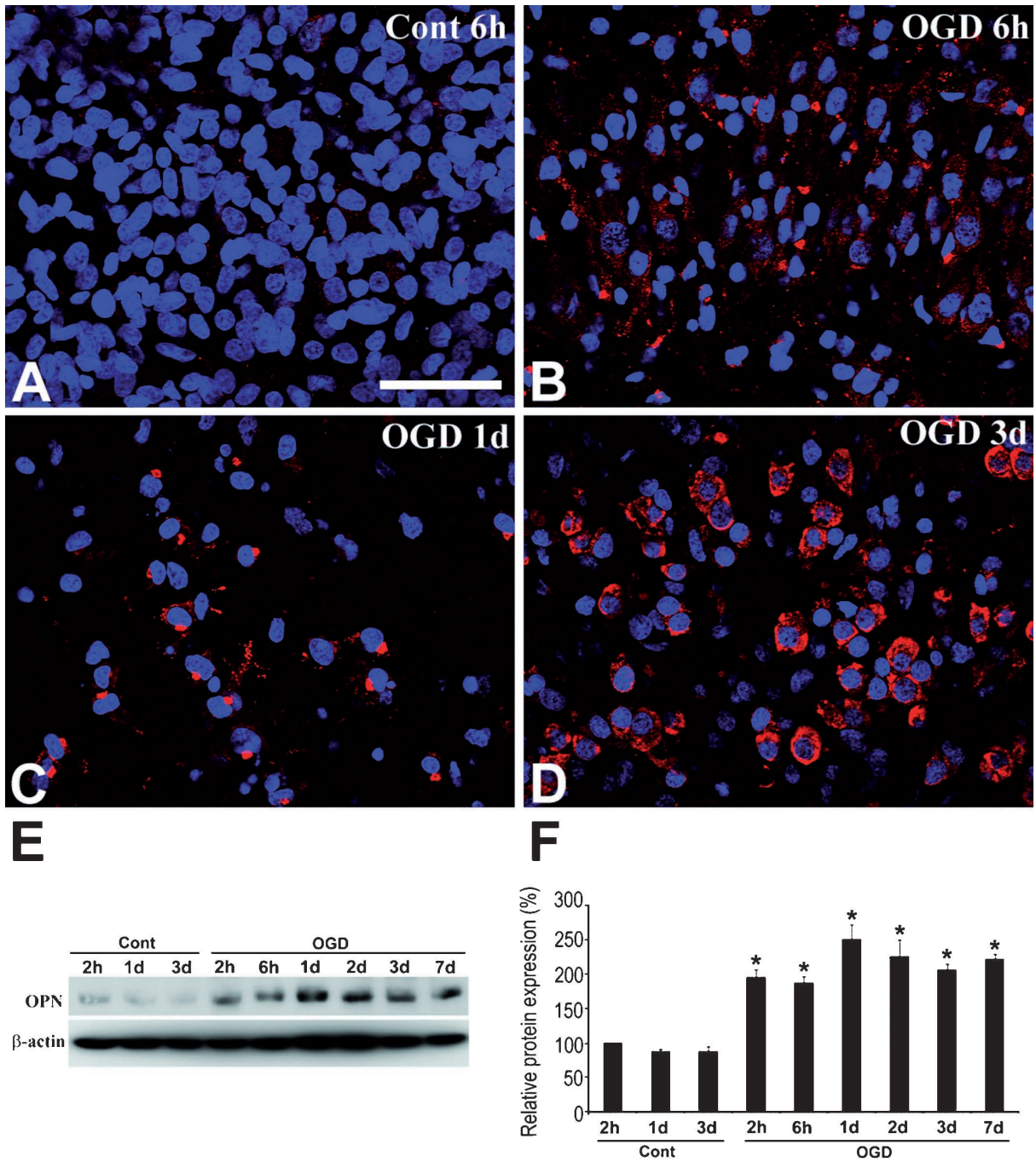

Fig. 4. Temporal changes in OPN immunoreactivity in the CA1 region in organotypic hippocampal slice cultures under control and OGD conditions. (A) At 6 h after sham-OGD, no significant basal expression of OPN protein was detected in the hippocampal CA1 region. (B) At 6 h after OGD, weak OPN-labeled profiles exhibiting a puntate cytosolic pattern were predominant in the CA1 region, and some scattered cells with the OPN concentrated in focal deposits were observed. (C) At 24 h after OGD, intensely labeled profiles with the OPN concentrated in focal deposits were more pronounced in the CA1 region. (D) At day 3 after OGD, OPN-immunoreactive cells exhibiting perinuclear staining with a punctate cytosolic pattern of OPN, typical secreted proteins, were observed in the CA1 region. (E) Immunoblotting with specific antibody against OPN revealed that OGD caused an upregulation of OPN protein in hippocampal slices compared with control slices. The level of β-tubulin served as the control for protein loading. (F) Densitometric analysis of immunoblotting of OPN. Results are expressed as a percentage of sham-OGD controls. *P<0.05 *versus* controls. Scale bar is 50 μm for (A)–(D).

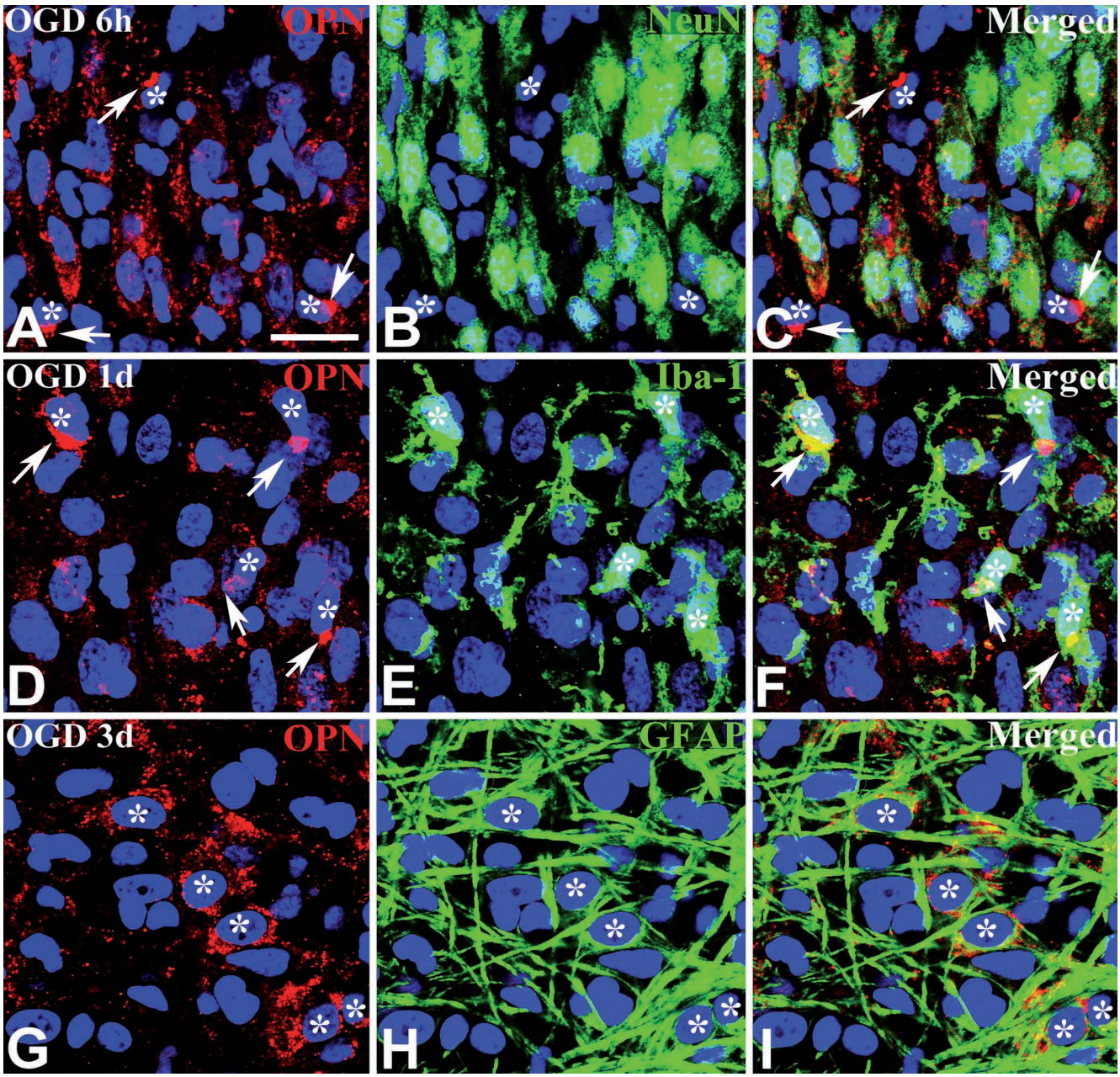

Fig. 5. Identification of phenotypes of OPN-immunoreactive cells in the CA1 pyramidal cell layer in organotypic hippocampal slice cultures at 6 h [(A)–(C)], day 1 [(D)–(F)] or day 3 [(G)–(I)] after OGD. [(A)–(C)] Double labeling for OPN protein (A) and NeuN (B) showed that weak immunoreactivity for OPN was observed in the neuronal cell body, whereas some cells [asterisks in (A)–(C)] showing OPN staining in focal sites [arrows in (A), (C)] were negative for NeuN. [(D)–(F)] Double labeling for OPN protein (D) and Iba-1 (E) revealed that OPN-immunoreactive cells demonstrating the OPN in focal deposits [arrows in (D), (F)] were indeed activated microglial cells [asterisks in (D)–(F)]. [(G)–(I)] Double labeling for OPN protein (G) and GFAP (H) revealed that most OPN-immunoreactive cells were GFAP-immunoreactive astrocytes [asterisks in (G)–(I)]. Scale bar is 20 μm for (A)–(I).

three days after OGD showed that OPN immunoreactivity appeared associated with a diffuse distribution in the cell bodies and almost all OPN-immunoreactive cells were reactive astrocytes (Fig. 5G–I).

DISCUSSION

The present study is the first to provide a detailed characterization of the time course of expression and

cellular phenotypes of OPN mRNA and protein in an *in vitro* model of stroke. OPN induction first occurred in CA1 pyramidal neurons as early as 2 h after OGD; however, OPN was absent in any neurons at day 1 after OGD. Instead, microglial cells began to express OPN at 6 h after OGD, and at day 2 after OGD the exclusive accumulation of OPN-expressing amoeboid-activated microglia was observed in the CA1 pyramidal cell layer, which correlates with the time points of microglial activation in oxygen-glucose-deprived hippocampal slice cultures (Chechneva et al. 2006). Considering that the hippocampal slice model used in this study contains only resident microglia and that an influx of peripheral leukocytes could not occur in this *in vitro* preparation, cells inducing OPN in the hippocampal slice culture after OGD should represent reactive microglial cells and not infiltrating blood-borne monocyte/macrophages. By day 3 after OGD, OPN was no longer expressed by microglial cells; however, astrocytes began to express OPN from then up to day 7 after OGD, which was the latest time point examined. These *in situ* hybridization and immunohistochemical observations were compatible with the post-OGD upregulation of OPN mRNA and protein in OHC, which were detected by semiquantitative RT–PCR analysis and immunoblotting, respectively. Overall, the sequential induction of OPN in microglia and astrocytes in early or late stages, respectively, in the ischemic hippocampal slice cultures is consistent with a previous report *in vivo* (Choi et al. 2007). This previous report showed that an early phase of acute microglial expression was followed by a delayed phase characterized by an induction of OPN in reactive astrocytes. Thus, our data from an *in vitro* model of stroke support this biphasic pattern of OPN expression *in vivo*, and suggest that OPN has a multifunctional role in the pathogenesis of ischemic injury.

Interestingly, contrary to the results of the observations *in vitro* others and we have demonstrated that there was no induction of OPN in pyramidal neurons in *in vivo* ischemic conditions (Ellison et al. 1998, 1999, Wang et al. 1998, Lee et al. 1999, Choi et al. 2007). Consequently, the results of the present *in vitro* study partially contrast with previous *in vivo* studies. Although the three-dimensional organization of the hippocampus is well preserved in culture conditions, slice cultures experience trauma, cell death, and deafferentation from extrahippocampal regions during slice preparation (Holopainen 2005, Noraberg et al. 2005). These differences to *in vivo* conditions may explain this discrepancy. However, the explanation for this discrepancy is not simple because the overall expression patterns between the *in vitro* and *in vivo* models are in excellent agreement. OGD induced death of CA1 pyramidal neurons within 2 h and dentate hilar neurons at day 1 after OGD in the *in vitro* model, which differs from global ischemia *in vivo* where initial cell death in the dentate hilus is followed by a delayed cell death in CA1 neurons at 2–4 days after OGD (Holopainen 2005, Noraberg et al. 2005). Therefore, this discrepancy might be related to the different patterns of neuronal cell death between *in vivo* and *in vitro* conditions.

Neuronal induction of OPN was rapid (within 2 h) and transient, and was mostly restricted to CA1 and CA3 pyramidal cells showing high susceptibility in response to OGD. At day 1 after OGD, no OPN expression was observed in preserved pyramidal neurons. Thus, neuronal OPN induction in OGD-induced hippocampal slice cultures is likely to represent a response to neuronal damage, at least in part, based on previous studies showing OPN upregulation in degenerating neurons (Chabas et al. 2001, Shin et al. 2005, Borges et al. 2008). However, it remains to be fully elucidated why the transient upregulation of OPN occurs in highly vulnerable CA1 and CA3 neurons after OGD.

Another issue that should be addressed is why OPN immunoreactivity localized to focal deposits in microglial cells, which appeared to be different from neurons and reactive astrocytes showing perinuclear staining with a punctate cytosolic pattern of OPN, typical of secreted proteins. These results are consistent with our previous reports *in vivo* (Choi et al. 2007, Kang et al. 2008), supporting the use of this system for morphological studies relating to the role of OPN in neurodegenerative diseases. Interestingly, several studies have identified an intracellular form of OPN that localized in perimembranous foci in activated macrophages, osteoclasts and fibroblasts, and it has been implicated in a number of cellular processes, including migration, fusion, and motility (Zohar et al. 2000, Chellaiah and Hruska 2002, Suzuki et al. 2002, Zhu et al. 2004). Therefore, our data from an *in vitro* model of stroke demonstrate that cellular localization of OPN protein appears to be cell-specific, and suggest that reactive astrocytes and activated microglial cells in response to OGD may express secreted OPN and an intracellular form of OPN, respectively.

CONCLUSIONS

Our study shows the sequential induction pattern of OPN expression in hippocampal slice cultures after OGD. The early response consisted of neuronal and microglial OPN upregulation, followed by a later extended phase of expression in reactive astrocytes. Activated microglia revealed OPN staining in focal sites, whereas neurons and reactive astrocytes showed perinuclear staining with a punctate cytosolic pattern of OPN, typical of secreted proteins.

The temporal and cellular patterns of OPN induction in reactive glial cells in this *in vitro* model closely correlate with that in the *in vivo* model. Thus, use of this system should permit advances in the understanding of the role of OPN in neurodegenerative diseases.

ACKNOWLEDGEMENT

This work was supported by Basic Science Research Program through the National Research Foundation of Korea (NRF) funded by the Ministry of Education, Science and Technology (No. 20090078886).

REFERENCES

Borges K, Gearing M, Rittling S, Sorensen ES, Kotloski R, Denhardt ET, Dingledine R (2008) Characterization of osteopontin expression and function after status epilepticus. Epilepsia 49: 1675–1685.

Chabas D, Baranzini SE, Mitchell D, Bernard CC, Rittling SR, Denhardt DT, Sobel RA, Lock C, Karpuj M, Pedotti R, Heller R, Oksenberg JR, Steinman L (2001) The influence of the proinflammatory cytokine, osteopontin, on autoimmune demyelinating disease. Science 294: 1731–1735.

Chechneva O, Dinkel K, Cavaliere F, Martinez-Sanchez M, Reymann KG (2006) Anti-inflammatory treatment in oxygen-glucose-deprived hippocampal slice cultures is neuroprotective and associated with reduced cell proliferation and intact neurogenesis. Neurobiol Dis 23: 247–259.

Choi JS, Kim HY, Cha JH, Choi JY, Lee MY (2007) Transient microglial and prolonged astroglial upregulation of osteopontin following transient forebrain ischemia in rats. Brain Res 1151: 195–202.

Chellaiah MA, Hruska KA (2002) The integrin $\alpha_v\beta_3$ and CD44 regulate the actions of osteopontin on osteoclast motility. Calcif Tissue Int 72: 197–205.

Doyle KP, Yang T, Lessov NS, Ciesielski TM, Stevens SL, Simon RP, King JS, Stenzel-Poore MP (2008) Nasal administration of osteopontin peptide mimetics confers neuroprotection in stroke. J Cereb Blood Flow Metab 28: 1235–1248.

Ellison JA, Velier JJ, Spera P, Jonak ZI, Wang X, Barone FC, Feuerstein GZ (1998) Osteopontin and its integrin receptor alpha$_v$beta$_3$ are upregulated during formation of the glial scar after focal stroke. Stroke 29: 1698–1707.

Ellison JA, Barone FC, Feuerstein GZ (1999) Matrix remodeling after stroke. De novo expression of matrix proteins and integrin receptors. Ann N Y Acad Sci 890: 204–222.

Holopainen IE (2005) Organotypic hippocampal slice cultures: a model system to study basic cellular and molecular mechanisms of neuronal cell death, neuroprotection, and synaptic plasticity. Neurochem Res 30: 1521–1528.

Kang WS, Choi JS, Shin YJ, Kim HY, Cha JH, Lee JY, Chun MH, Lee MY (2008) Differential regulation of osteopontin receptors, CD44 and the alpha(v) and beta(3) integrin subunits, in the rat hippocampus following transient forebrain ischemia. Brain Res 1228: 208–216.

Laake JH, Haug FM, Wieloch T, Ottersen OP (1999) A simple in vitro model of ischemia based on hippocampal slice cultures and propidium iodide fluorescence. Brain Res Protoc 4: 173–184.

Lee MY, Shin SL, Choi YS, Kim EJ, Cha JH, Chun MH, Lee SB, Kim SY (1999) Transient upregulation of osteopontin mRNA in hippocampus and striatum following global forebrain ischemia in rats. Neurosci Lett 271: 81–84.

Maetzler W, Berg D, Schalamberidze N, Melms A, Schott K, Mueller JC, Liaw L, Gasser T, Nitsch C (2007) Osteopontin is elevated in Parkinson's disease and its absence leads to reduced neurodegeneration in the MPTP model. Neurobiol Dis 25: 473–482.

Meller R, Stevens SL, Minami M, Cameron JA, King S, Rosenzweig H, Doyle K, Lessov NS, Simon RP, Stenzel-Poore MP (2005) Neuroprotection by osteopontin in stroke. J Cereb Blood Flow Metab 25: 217–225.

Noraberg J, Poulsen FR, Blaabjerg M, Kristensen BW, Bonde C, Montero M, Meyer M, Gramsbergen JB, Zimmer J (2005) Organotypic hippocampal slice cultures for studies of brain damage, neuroprotection and neurorepair. Curr Drug Targets CNS Neurol Disord 4: 435–452.

Schroeter M, Zickler P, Denhardt DT, Hartung HP, Jander S (2006) Increased thalamic neurodegeneration following ischaemic cortical stroke in osteopontin-deficient mice. Brain 129: 1426–1437.

Shin T, Ahn M, Kim H, Moon C, Kang TY, Lee JM, Sim KB, Hyun JW (2005) Temporal expression of osteopontin

and CD44 in rat brains with experimental cryolesions. Brain Res 11: 95–101.

Stoppini L, Buchs PA, Muller D (1991) A simple method for organotypic cultures of nervous tissue. J Neurosci Methods 37: 173–182.

Suzuki K, Zhu B, Rittling SR, Denhardt DT, Goldberg HA, McCulloch CA, Sodek J (2002) Colocalization of intracellular osteopontin with CD44 is associated with migration, cell fusion, and resorption in osteoclasts. J Bone Miner Res 17: 1486–1497.

Wang X, Louden C, Yue TL, Ellison JA, Barone FC, Solleveld HA, Feuerstein GZ (1998) Delayed expression of osteopontin after focal stroke in the rat. J Neurosci 18: 2075–2083.

Zhu B, Suzuki K, Goldberg HA, Rittling SR, Denhardt DT, McCulloch CA, Sodek J (2004) Osteopontin modulates CD44-dependent chemotaxis of peritoneal macrophages through G-protein-coupled receptors: evidence of a role for an intracellular form of osteopontin. J Cell Physiol 198: 155–167.

Zohar R, Suzuki N, Suzuki K, Arora P, Glogauer M, McCulloch CA, Sodek J (2000) Intracellular osteopontin is an integral component of the CD44-ERM complex involved in cell migration. J Cell Physiol 184: 118–130.